

Article

Preparation of C₃N₄ Thin Films for Photo-/Electrocatalytic CO₂ Reduction to Produce Liquid Hydrocarbons

Jin You Zheng ^{1,*} , Amol Uttam Pawar ² and Young Soo Kang ^{2,*}

¹ Engineering Research Center of Advanced Functional Material Manufacturing of Ministry of Education, School of Chemical Engineering, Zhengzhou University, Zhengzhou 450001, China

² Environmental and Climate Technology, Korea Institute of Energy Technology, Naju-si 58219, Korea

* Correspondence: jinyouzh@zzu.edu.cn (J.Y.Z.); yskang@kentech.ac.kr (Y.S.K.)

Abstract: Thermal vapor condensation of melamine at various temperatures was used to fabricate thin graphitic carbon nitride (g-C₃N₄) films on fluorine-doped tin oxide (FTO) coated glass substrates. Photoanodic (n-type) and photocathodic (p-type) responses were observed simultaneously in the g-C₃N₄ films. The g-C₃N₄ film formed at 520 °C with the longest average lifetime of the photo-excited electrons shows the best cathodic photocurrent performance, which was then chosen for electrochemical and photoelectrochemical reduction of CO₂. When the basic electrolyte (CO₂-saturated 0.5 M KHCO₃, pH = 7.6) was adopted, CO₂ was electrochemically converted into formaldehyde ((54.6 μM/h)) in the liquid product. When the acidic electrolyte (CO₂-saturated 0.5 M KCl, pH = 4.1) was adopted, formaldehyde (39.5 μM/h) and ethanol (15.7 μM/h) were generated through photoelectrochemical reduction, stimulated by the presence of sufficient protons from the electrolyte in the reduction process. Therefore, the pure g-C₃N₄ film has a great potential for CO₂ reduction to value-added liquid hydrocarbons products via electrochemical or photoelectrochemical ways.

Keywords: graphitic carbon nitride; CO₂ reduction; thin film; photoelectrochemical property



Citation: Zheng, J.Y.; Pawar, A.U.; Kang, Y.S. Preparation of C₃N₄ Thin Films for Photo-/Electrocatalytic CO₂ Reduction to Produce Liquid Hydrocarbons. *Catalysts* **2022**, *12*, 1399. <https://doi.org/10.3390/catal12111399>

Academic Editor: Ali Seifitokaldani

Received: 26 September 2022

Accepted: 4 November 2022

Published: 9 November 2022

Publisher's Note: MDPI stays neutral with regard to jurisdictional claims in published maps and institutional affiliations.



Copyright: © 2022 by the authors. Licensee MDPI, Basel, Switzerland. This article is an open access article distributed under the terms and conditions of the Creative Commons Attribution (CC BY) license (<https://creativecommons.org/licenses/by/4.0/>).

1. Introduction

Conversion of carbon dioxide (CO₂) to value-added chemicals, such as methanol (CH₃OH), ethanol (C₂H₅OH), formic acid (HCOOH), methane (CH₄), carbon monoxide (CO), etc., is one of the best way of carbon capture and utilization (CCU) to solve the energy and environmental issues [1,2]. The process has been reported being achieved by chemical methods, photocatalytic reduction, electrocatalytic reduction, photoelectrocatalytic reduction, and a few other strategies [1]. Particularly, photoelectrocatalytic CO₂ reduction has several advantages such as directly utilizing the solar energy and is an effective control on the reduction products by changing the experimental parameters, such as temperature, electrolyte, applied potential, etc. [3]. Polymeric graphitic carbon nitride (g-C₃N₄, denoted as CN), a metal-free polymetric semiconductor with band gap of ca. 2.7 eV, has attracted much research attention for its potential to be the next generation of superior photocatalyst, due to its nontoxicity, low cost, facile synthesis, appealing electronic band structure and high physicochemical stability [4–7]. g-C₃N₄ is thermally stable up to about 600 °C in air and chemically stable in acid, alkali, or organic solvents [8–10]. g-C₃N₄-based nanocomposites have been widely reported for degradation of pollutants and bacterial disinfection, water splitting for H₂ and O₂ evolution, and photocatalytic/photoelectrocatalytic/photothermal reduction of CO₂ into hydrocarbon fuels [4–7,11–15]. Specially, the N–C=N-binding motifs in g-C₃N₄ can fix CO₂ as a carbamate and catalyze the reactions involving CO₂ [11,16,17].

For g-C₃N₄ used for CO₂ reduction, most recent works were related to photocatalysis with g-C₃N₄-based photocatalysts [4,7]. However, the photocatalytic activity of pure g-C₃N₄ has relatively low efficiency due to its low potential for water oxidation that is a counter reaction in the process of CO₂ reduction [16]. Comparatively, the photoelectrochemical

(PEC) method is an improved strategy for CO₂ reduction (g-C₃N₄ as cathode or photocathode) since the external bias can strongly drive the water oxidation reaction. Several works related to g-C₃N₄-based photocathodes, such as B-doped g-C₃N₄ [16], Au loaded B-doped g-C₃N₄ [16], Co-porphyrin/g-C₃N₄ [18], Pd/Ti₃C₂/g-C₃N₄ [19], g-C₃N₄/ZnTe [20], Pd/Cu/g-C₃N₄NTs [21], CuO/g-C₃N₄ [22], have been reported on PEC CO₂ reduction. The reported reduction products range from liquid to gas phases, including C₂H₅OH, CH₃OH, HCOOH, C₃H₇OH, CH₄, CO, H₂, etc. [7,15]. Generally, compared with the nanoparticle materials, g-C₃N₄ in the form of thin film has a low degree of crystallinity and a high degree of electron-hole recombination. Therefore, despite low electrocatalytic efficiency, pure g-C₃N₄ films are good candidates for investigating the fundamental process of CO₂ reduction based on g-C₃N₄ materials.

Herein, thin g-C₃N₄ films have been fabricated on FTO glass substrates by simple thermal vapor condensation of melamine at various heating temperatures. Interestingly, these films show both photoanodic (n-type) and photocathodic (p-type) properties. The film formed at 520 °C, in particular, has the best cathodic photocurrent performance. It was chosen for investigation into CO₂ reduction electrochemically and photoelectrochemically. When utilizing a basic electrolyte (CO₂-saturated KHCO₃), CO₂ is electrochemically converted to formaldehyde in the liquid product. When utilizing an acidic electrolyte (CO₂-saturated KCl), ethanol may also be generated through photoelectrochemical reduction, which could be due to the presence of sufficient protons in the CO₂ reduction process. The g-C₃N₄ films give a great potential for CO₂ reduction to value-added hydrocarbons products via electrochemical or photoelectrochemical ways.

2. Results and Discussion

By heating, the precursors such as cyanamide, dicyanamide, melamine, urea, thiourea, and ammonium thiocyanate, can easily form g-C₃N₄ [4]. In this work, the melamine was selected as a precursor for synthesis of g-C₃N₄ films. Undergoing condensation reactions with elimination of ammonia, the melamine can transfer to melem at ca. 390 °C and to melon at >500 °C, and finally become g-C₃N₄ at ca. 520 °C as shown in Figure 1 [23]. After thermal vapor condensation reaction of melamine, the thin g-C₃N₄ films can be uniformly deposited on FTO glass surface at 520 °C, 550 °C, and 600 °C (denoted as CN/FTO-520, CN/FTO-550, and CN/FTO-600, respectively) as the scanning electron microscope (SEM) images shown in Figure 2. SnO₂ particles can be easily observed in the bare FTO films (Figure S1). The FTO surface is fully covered by a g-C₃N₄ layer with a thickness of ca. 70 nm at 520 °C. As the temperature was increased to 550 °C and 600 °C, the surface roughness of the films becomes less and the thickness of the films becomes much thinner. Especially, the film obtained at 600 °C is very thin; it is easy to determine the SnO₂ crystals under the bottom of the g-C₃N₄ film. The thicknesses of CN/FTO-550 and CN/FTO-600 are around 34 nm and 27 nm, respectively. The thickness of g-C₃N₄ films becomes thinner as the increase of heating temperature. At a higher heat temperature, the temperature of FTO substrate will be also higher; the deposition rate becomes slow while the evaporation rate becomes high. Therefore, the thickness of film obtained at high temperature will be thinner than the film obtained at low temperature. Since the films are very thin, their crystal structures (characteristic peak of (002)) and crystallinities cannot be detected by X-ray diffraction (XRD) as shown in Figure 3a. The powder samples obtained at same condition with the preparation of film are g-C₃N₄, which are confirmed by XRD (Figure 3c,d). Especially, as the heating temperature is increased, the 2θ position of (002) peak shifts to large values such as 27.62° for CN-520, 27.68 for CN-550, and 27.76 for CN-600, which are corresponding to the *d*-spacing values of 3.2269 Å, 3.2201 Å, and 3.2110 Å, respectively. The (002) plane is attributed to the interlayer stacking of aromatic segments. This stacking in g-C₃N₄ is tighter than the packing than graphene (*d* = 3.53 Å) and crystalline graphite (*d* = 3.35 Å), which is attributed to the more localization of the electrons and strong binding between the layers by heteroatom substitution [11,23]. As the

temperature increases, the d -spacing of the g - C_3N_4 becomes shorter, which is indicating more dense packing of the g - C_3N_4 layers [23].

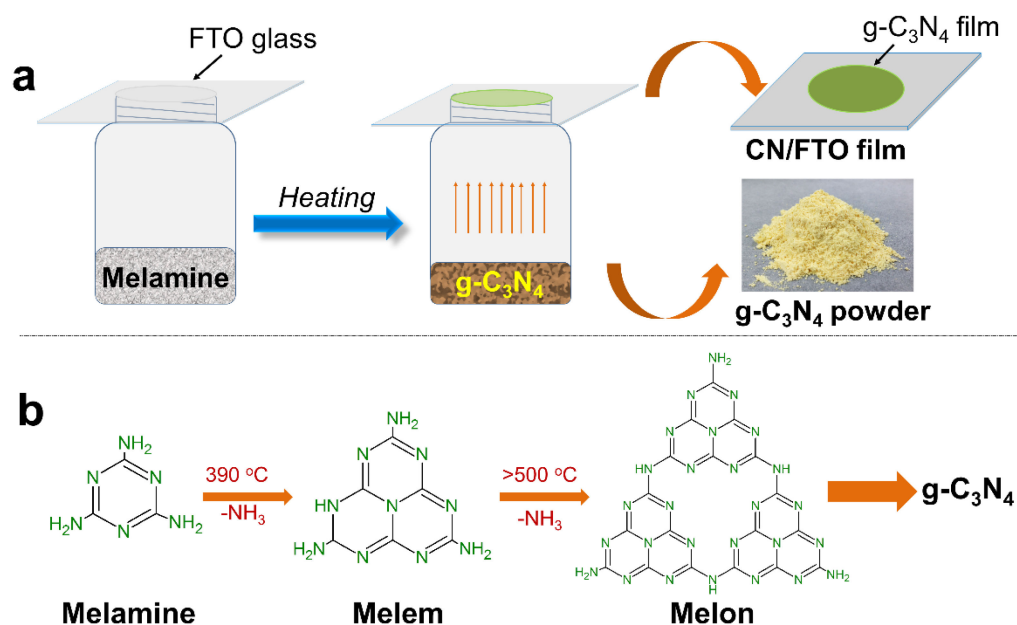


Figure 1. Schematic illustration of (a) the experimental procedure for preparing thin CN/FTO film and g - C_3N_4 powder samples via heating melamine precursor, and (b) thermal polymerization of melamine to g - C_3N_4 .

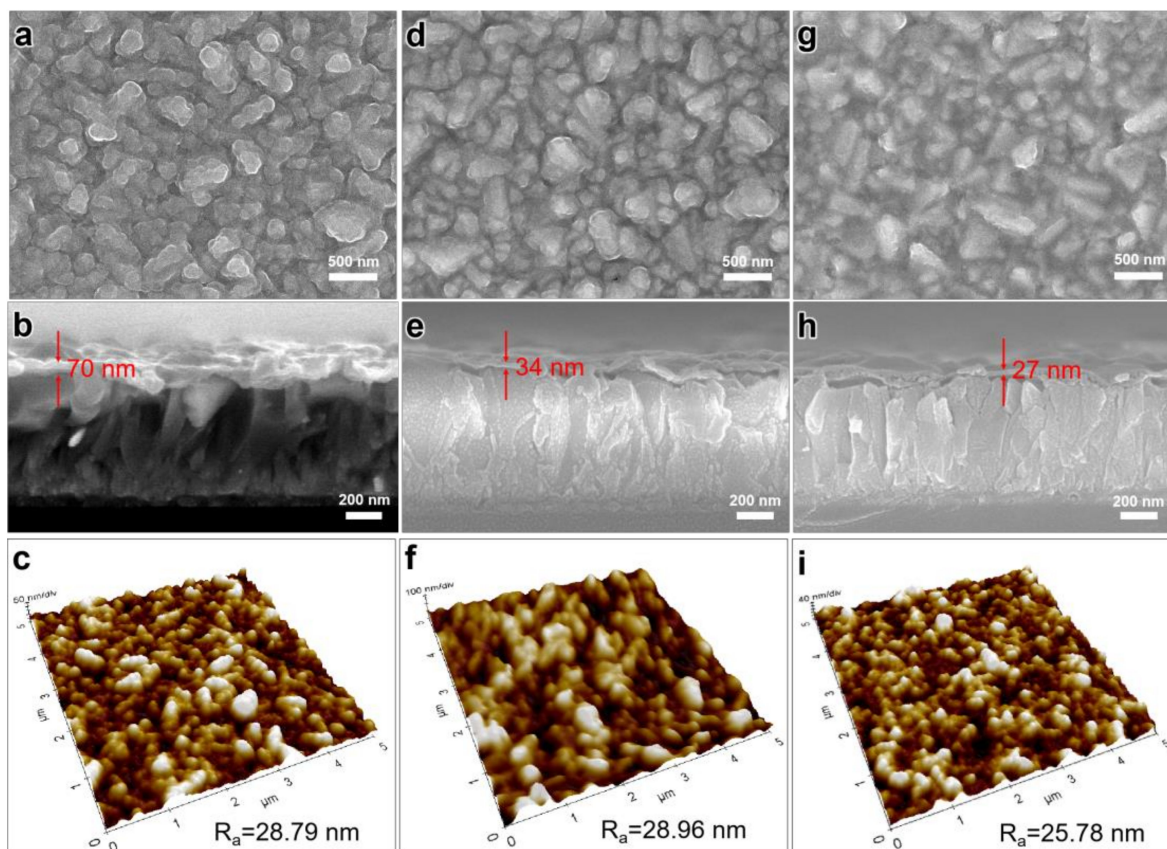


Figure 2. Top-view, cross-sectional SEM and AFM images of (a–c) CN/FTO-520, (d–f) CN/FTO-550, and (g–i) CN/FTO-600.

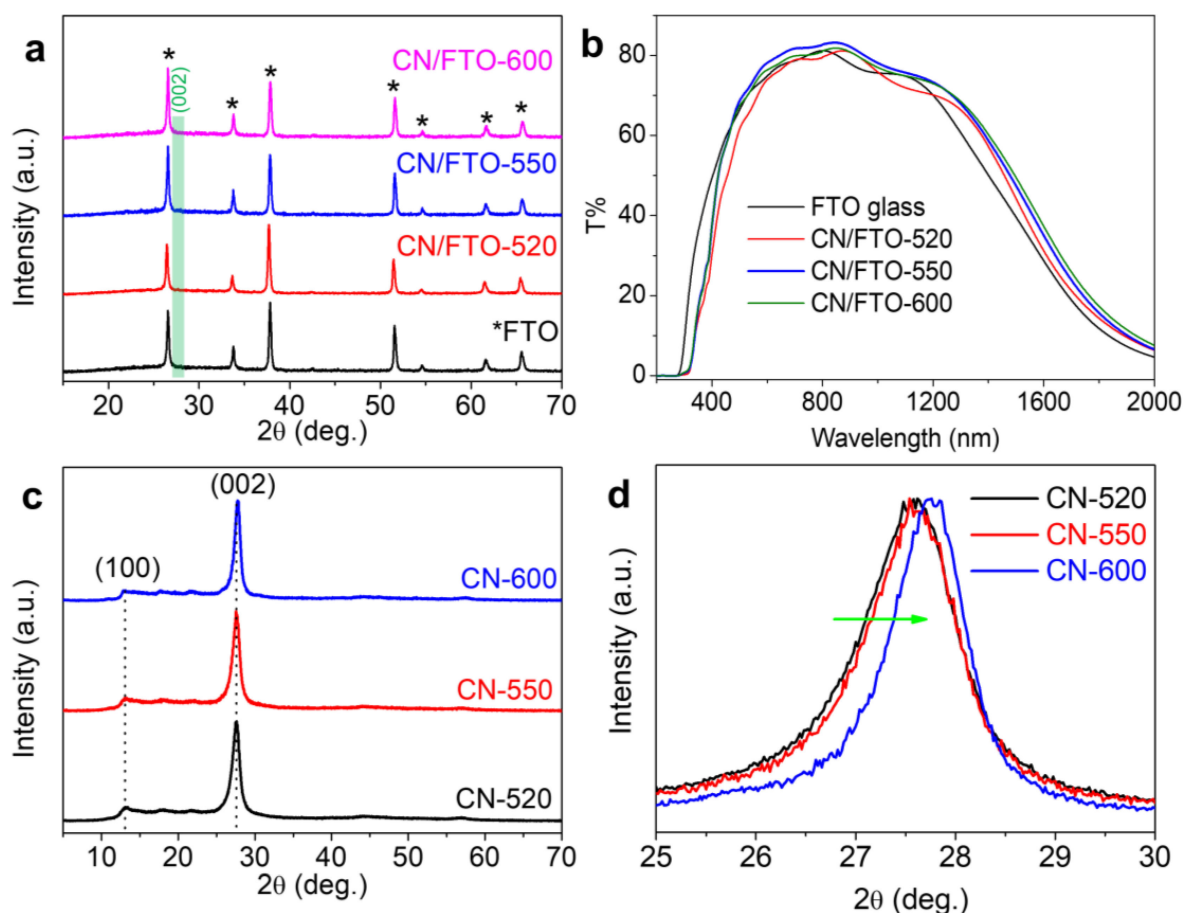


Figure 3. (a) XRD patterns and (b) transmittances of CN/FTO films. (c) CN powders obtained at 520, 550, and 600 °C. (d) Overlap XRD patterns to show the peak shifting.

To show the optical properties, the transmittance of the CN/FTO films synthesized at different temperatures was measured by UV-vis-NIR spectroscopy in the wavelength range of 400 to 2000 nm as shown in Figure 3b. Since the films are very thin, their transmittances are very similar and even better than the transmittance of the bare FTO substrate in some range of wavelength. Since the FTO surface is very rough ($R_a = 30.78$ nm, Figure S1b) and has clear crystal facets, the reflectance of light is serious [24,25]. After deposition of $g\text{-C}_3\text{N}_4$ thin films on FTO surface, the roughness of film become smaller as the Atomic force microscopy (AFM) results shown in Figure 2c,f,i. The average roughness of CN/FTO-520, CN/FTO-550, and CN/FTO-600 are 28.79 nm, 28.96 nm, and 25.78 nm, respectively. In addition, the surface of $g\text{-C}_3\text{N}_4$ film has no clear crystal facet, thus the reflectance of light is relatively weak. Therefore, the transmittance of the CN/FTO-550 and CN/FTO-600 in the range of 470 to 2000 nm is better than that of the bare FTO substrate.

To know the components of the CN/FTO-520 film, energy-dispersive spectroscopy (EDS) was conducted as shown in Figure S2. Four kinds of elements, namely C, N, O, and Sn, were detected. C and N elements come from the $g\text{-C}_3\text{N}_4$ film; Sn and O elements come from FTO substrate. The elemental ratio of C:N is ca. 1:1, which is larger than the theoretical ratio of 3:4. It is so-called a C-rich $g\text{-C}_3\text{N}_4$ or C-doped $g\text{-C}_3\text{N}_4$. Generally, $g\text{-C}_3\text{N}_4$ is composed of condensed π -conjugated six-membered rings of triazine or tri-s-triazine (s-heptazine, C_6N_7) units bridged together with nitrogen atoms which give a two-dimensional graphitic structure [26,27]. For C-rich $g\text{-C}_3\text{N}_4$, a large number of delocalized π bonds are formed in $g\text{-C}_3\text{N}_4$ [27,28]. To know the detailed chemical composition and state of the typical CN/FTO-520 film, X-ray photoelectron spectroscopy (XPS) survey scan spectrum and C1s and N1s spectrum are shown in Figure 4. The survey scan spectrum shows only carbon and nitrogen elements, and no oxygen. It indicates that the $g\text{-C}_3\text{N}_4$ film is fully

covered on FTO glass. The C1s core-level spectrum can be deconvoluted into three main peaks with the binding energies at 284.6 eV, 286.29 eV, and 288.02 eV, which are assigned to sp^2 C–C bonds of graphitic carbon, sp^3 -coordinated carbon bonds, and sp^2 -bonded carbon in N–C=N of the s-triazine rings, respectively [14,29,30]. The bonding energy for C1s peak at 284.6 eV, used as the reference for calibration, can be attributed to the sample preparation (carbon sources in air) and subsequent handling, or the slightly exposed carbon tape which was used for holding samples [31]. N1s signal can be fitted with four peaks. Three main binding energies at 398.62 eV, 399.99 eV, and 400.96 eV are corresponding to the sp^2 -bonded N of C–N=C, tertiary nitrogen N–(C)₃ groups and amino groups of C–N–H [14,29,30]. The minor peak at 404.29 eV is attributed to the charge effects or positive charge localization in heterocycles due to π -excitations [23,32]. XPS data show that the pure g-C₃N₄ films were obtained and fully covered on FTO glass.

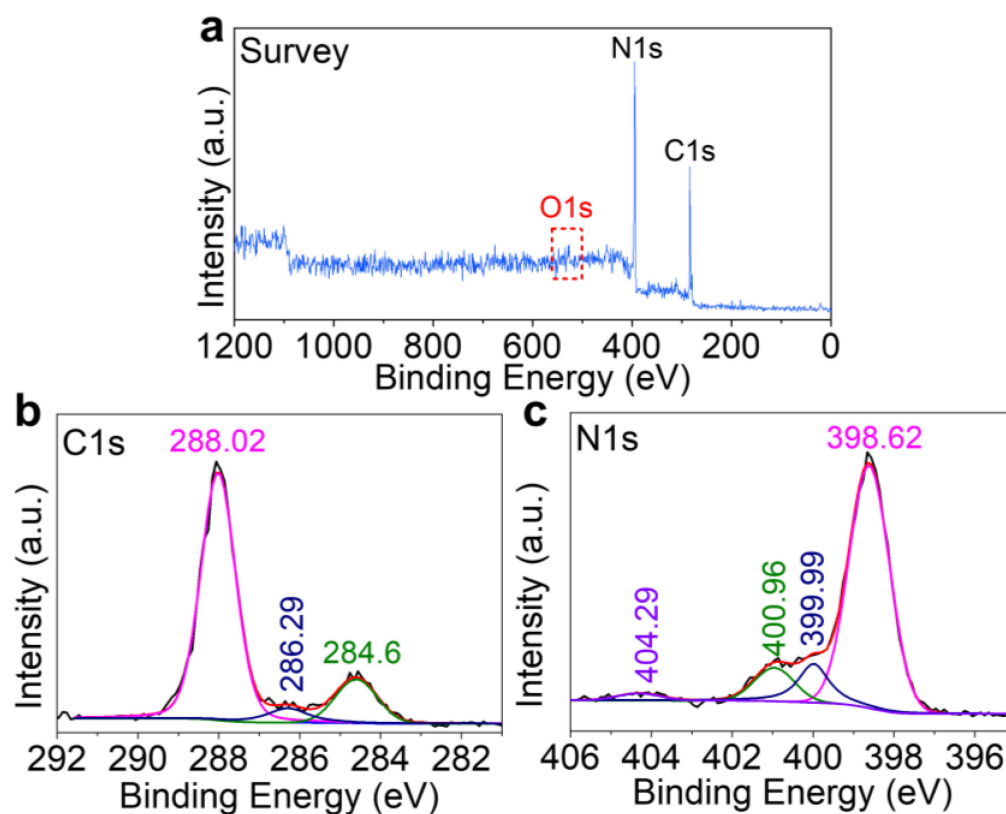


Figure 4. XPS spectra of CN/FTO-520 film: (a) survey scan, (b) C1s and (c) N1s.

To know the detailed chemical structures of the g-C₃N₄ films, the Attenuated total reflectance Fourier transform infrared spectroscopy (ATR-FTIR) spectra of melamine precursor, g-C₃N₄ powder, FTO substrate and CN/FTO films obtained at different heating temperature were measured in the wavenumber range of 650 to 4000 cm^{-1} as shown in Figure 5. IR spectrum of the bare FTO substrate did not show any peak. Thus, all the peaks of CN/FTO films should come from the g-C₃N₄ thin film rather than the FTO substrate. The results are very similar to previous reports [23,33]. The sharp absorption peaks for melamine (810 cm^{-1}), CN-520 powder (804 cm^{-1}) and CN/FTO films (822 cm^{-1}) are assigned to the breathing mode of triazine units [11,23]. The peaks of g-C₃N₄ powder and CN/FTO films in the range of 1198 to 1626 cm^{-1} are corresponding to the characteristic stretching modes of C–N heterocycles [23,33,34]. The broad peaks in the wavenumber range of 3000 to 3500 cm^{-1} are contributed to the N–H stretching from residual –NH₂ groups and the –OH band from the physically adsorbed H₂O molecules [23,35,36].

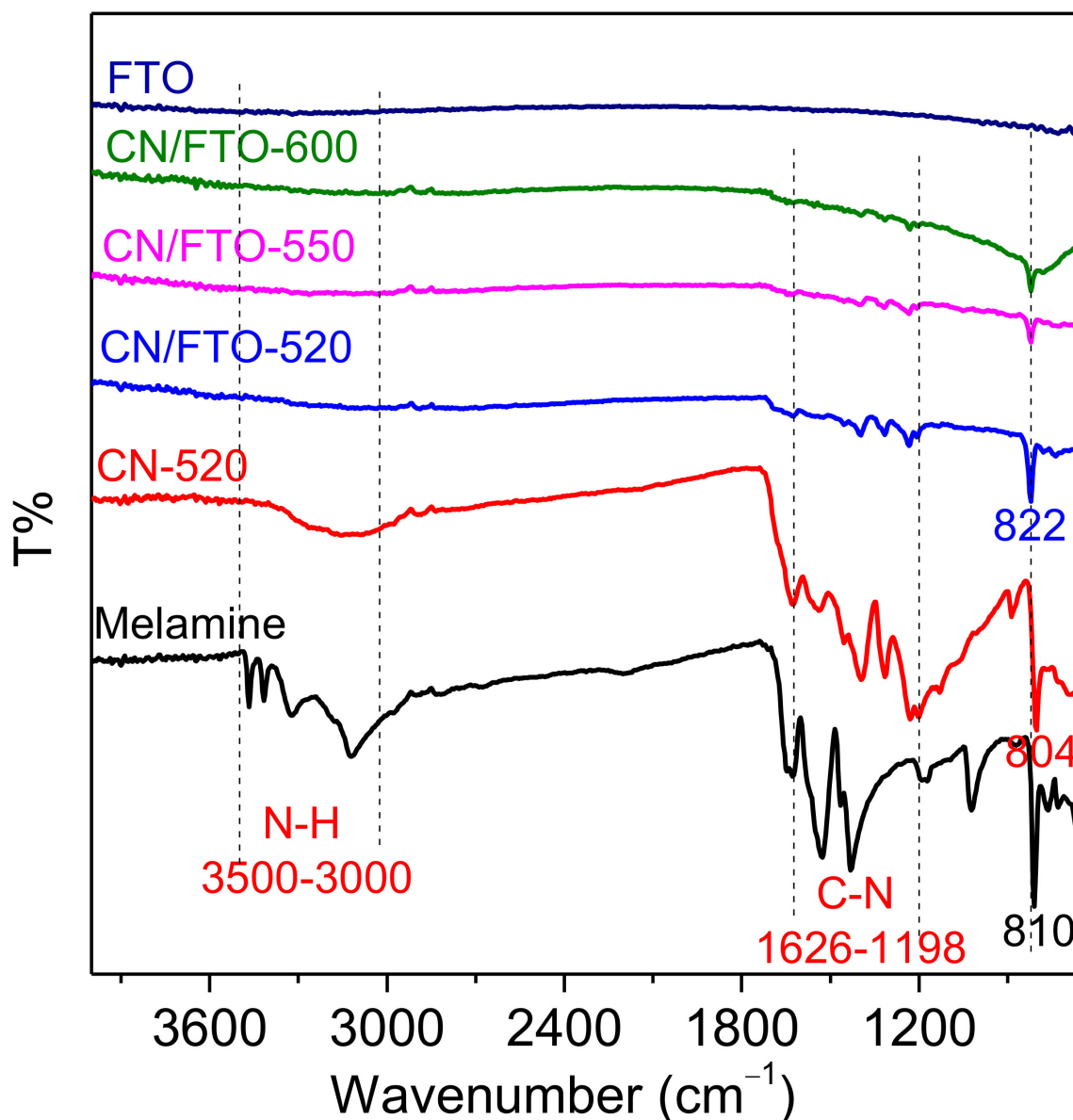


Figure 5. ATR-FTIR spectra of pure melamine and typical g-C₃N₄ powder (CN-520), FTO substrate, and CN/FTO films.

To indicate the distribution and the average lifetime of the photo-excited electrons on different electrodes, the time-resolved photoluminescence (TPRL) images and lifetime decay curves are measured as shown in Figure 6. The bare FTO substrate shows no photo-excited electrons; its effect on g-C₃N₄ film can be ignored. According the colors and contrast of the CN/FTO films, all films show that the photo-generated electrons are uniformly distributed on the surface of each electrode. It directly indicates all films are prepared uniformly. To know the average fluorescence lifetimes of films, the fluorescence lifetimes were calculated by fitting the fluorescence decay to a bi-exponential function as shown in Figure S3. The corresponding intensity-weighted average lifetime is shown as the inset in Figure 6e. The average lifetimes for the films obtained at 520 °C, 550 °C, and 600 °C are 3.90 ns, 3.82 ns, and 3.12 ns, respectively, as shown in Table S1. The film obtained at 520 °C shows the longest lifetime. Therefore, the CN/FTO-520 film can have better photo-catalytic property compared with the other two films. Thus, we choose the CN/FTO film for photoelectrochemical CO₂ reduction.

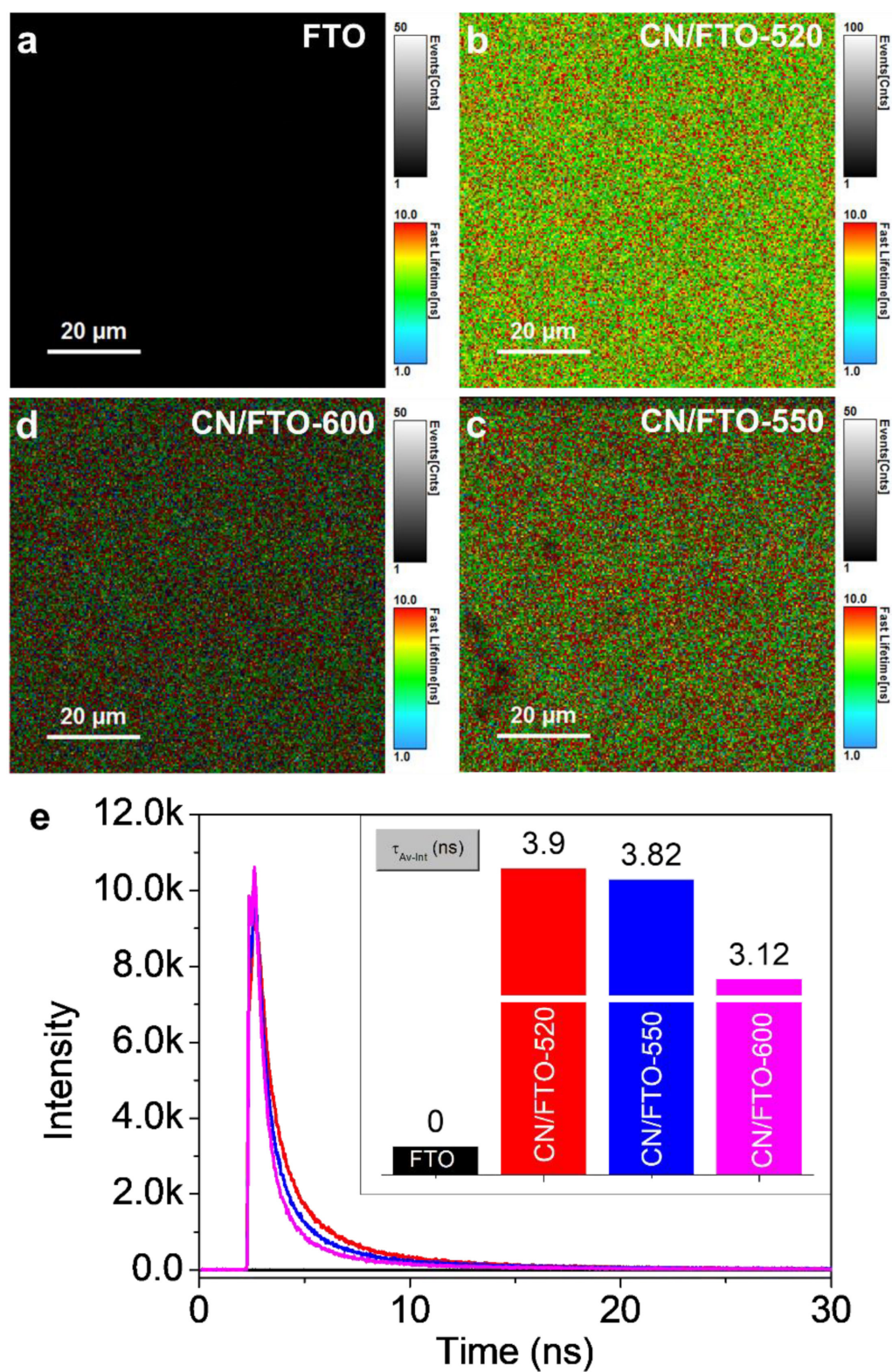


Figure 6. Time-resolved photoluminescence (TRPL) images of (a) bare FTO, (b) CN/FTO-520, (c) CN/FTO-550, (d) CN/FTO-600 films and (e) their decay curves. Inset of (e) are the corresponding intensity-weighted average lifetimes of different films.

For a semiconductor material, its optical absorption and band gap energy are very important for its photochemical or photoelectrochemical performance. Therefore, the optical absorption of the prepared films and the bare FTO glass substrate measured by UV-vis diffuse reflectance spectra (DRS). All CN/FTO films have the similar absorption edge at ca. 430 nm as shown in Figure 7a. The indirect band gap energies were extracted for CN/FTO films by plotting $(F(R)hv)^{1/2}$ vs. hv as shown in Figure 7b. The indirect allowed band gap energies for all CN/FTO films are ca. 2.89 eV. The pure g-C₃N₄ films can show only anodic photocurrent [36–39], only cathodic photocurrent [40,41], and both anodic and cathodic photocurrents [42,43] depending on the different precursors and preparation method of the films. I–V scanning curves from 1.5 V to –0.25 V vs. RHE show both the photoanodic and photocathodic characteristics at plus potential and negative potential range, respectively, as shown in Figure 7c. The photocurrent switch potential is around 0.66 V_{RHE}. The detailed anodic photocurrent (1.5 to 0.66 V_{RHE}) and cathodic photocurrent (0.66 to –0.25 V_{RHE}) performances are shown in Figure 7d,e. The CN/FTO-600 film has the best anodic photocurrent with photocurrent density of 0.72 μA/cm² at 1.23 V_{RHE} while the CN/FTO-520 film has the best cathodic photocurrent density of 1.1 μA/cm² at 0 V_{RHE}. To know the reason for the different photocurrent performances of different electrodes, their interfacial charge-transfer resistances (R_{ct}) are measured at E_{oc} by EIS Nyquist plots under dark as shown in Figure 7f [31]. All three films show very high charge-transfer resistances since the diameter of arc radius are huge. The order of R_{ct} for these three films is $R_{ct-600} < R_{ct-520} < R_{ct-550}$. This order of R_{ct} is matched with the performance of anodic photocurrent at 1.23 V_{RHE}. The CN/FTO-520 film with best cathodic photocurrent performance is chosen for CO₂ reduction. To check the stability of the CN/FTO-520 film, the cyclic voltammograms are checked with 10 cycles under 1 sun light illumination as shown in Figure 7g. There is no obvious change, which indicates the CN/FTO film is very stable with applied bias and under light illumination. In addition, the photoelectrochemical stability were also confirmed by photocurrent vs. time curves, which were also checked at 1.18 V_{RHE} and 0.38 V_{RHE} for 1 h under 1 sun light illumination as shown in Figure 7h.

According to previous published work from our lab, the poly(4-vinylpyridine) electrode was used for electrochemical CO₂ and the main product is formaldehyde since the pyridine groups [44]. Since the g-C₃N₄ film is also including the similar functional group, it is expected that the main product could be formaldehyde. Therefore, the CN/FTO films were used for CO₂ reduction by the electrochemical method at different applied potentials of –0.042 V, –0.242 V, and –0.442 V vs. RHE in CO₂-saturated 0.5 M KHCO₃. The GC spectra and their corresponding concentrations are shown in Figure 8. At –0.042 V_{RHE} for 3 h, the main product concentration of formaldehyde is ca. 163.7 μmol/L. As the applied potential was increased to –0.242 V_{RHE} and –0.442 V_{RHE}, the concentration of formaldehyde is decreased. The main reason is that H₂ is preferred at more negative potential. The similar phenomenon was obtained by using the poly(4-vinylpyridine) electrode [44]. When the applied potential was increased to –0.842 V_{RHE}, the CN/FTO film was damaged and the FTO film was reduced to Sn metal particles as shown in Figure S4a. The corresponding XRD pattern confirms that the Sn metal is formed on the surface of FTO as shown in Figure S4b. In addition, the STEM-EDS mapping images (Figure S4c) give direct evidence that Sn nanoparticles are formed. Thus, the CN/FTO film is not stable at too negative potential such as the potential less than –0.842 V_{RHE}. However, Sn metal is also a good electrochemical catalyst; it can be used for the electrochemical reduction of CO₂ to formate (HCOO[–]) and CO [45–48]. Further work related to the direct reduction of FTO glass to Sn film for CO₂ reduction can be studied.

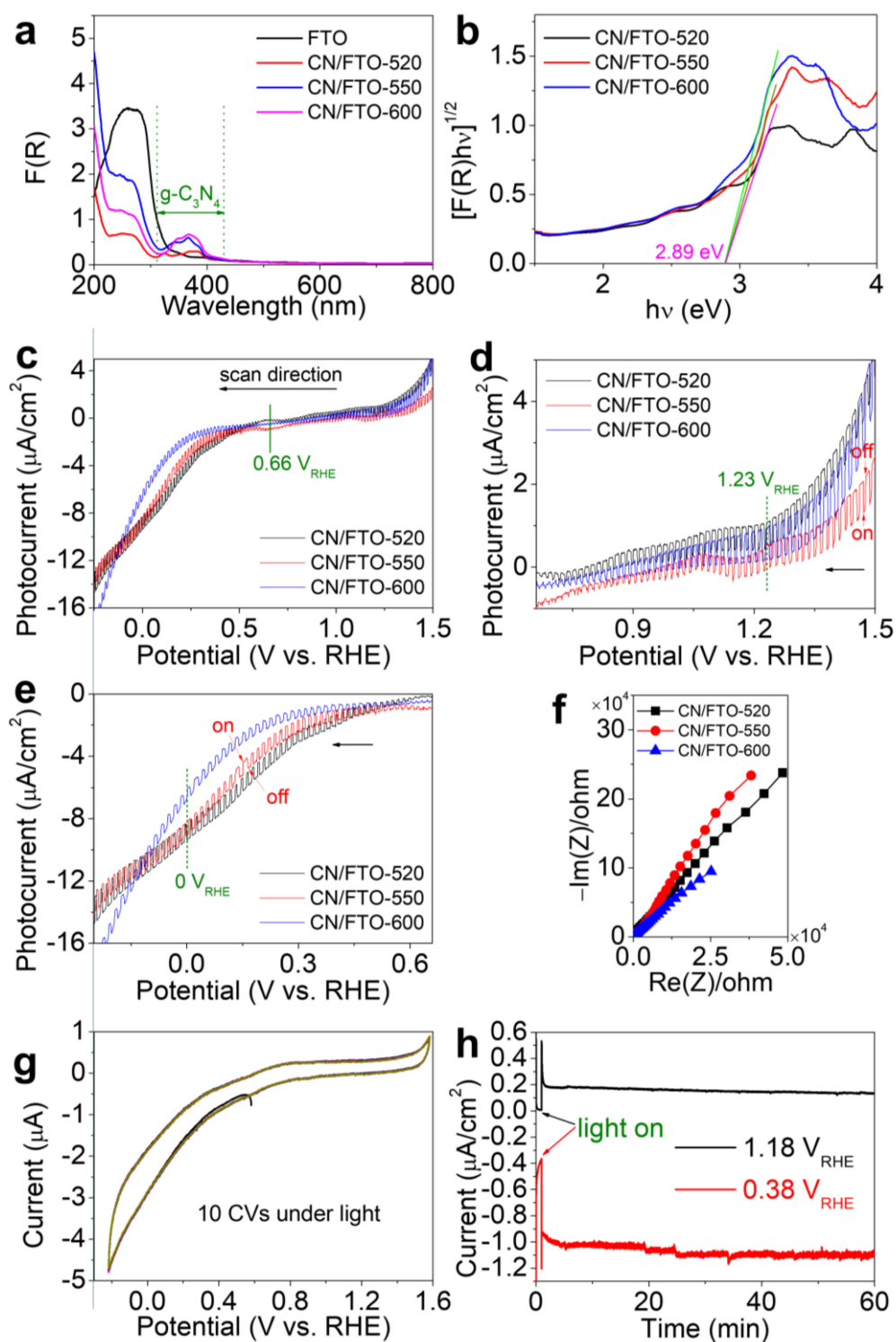


Figure 7. (a) DRS and (b) their corresponding Tauc plots ($(F(R)hv)^{1/2}$ versus $h\nu$ for the indirect band gap), photocurrent I–V curves (c) from 1.5 to $-0.25 V_{RHE}$, (d) from 1.5 to $0.66 V_{RHE}$, and (e) from 0.66 to $-0.25 V_{RHE}$, (f) EIS spectra of CN/FTO-520, CN/FTO-550, and CN/FTO-600 films. (g) Cyclic voltammograms of CN/FTO-520 under 1 sun light illumination. (h) Photoelectrochemical stabilities of CN/FTO-520 film checked at $1.18 V_{RHE}$ and $0.38 V_{RHE}$ for 1 h.

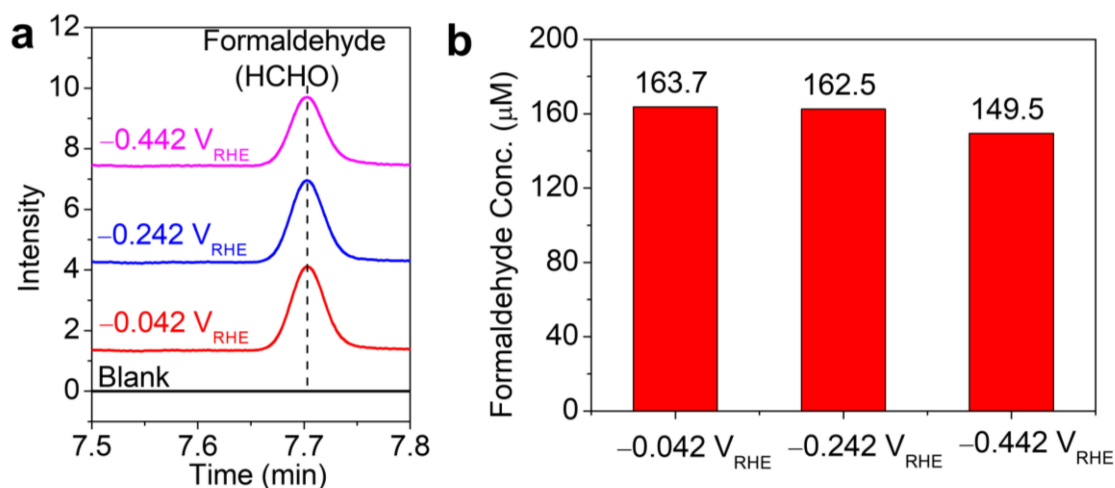


Figure 8. (a) GC spectra and (b) the corresponding product concentration for electrochemical CO_2 reduction by CN/FTO-520 film in CO_2 -saturated 0.5 M KHCO_3 solution at different applied potentials for 3 h.

As shown in Figure 9a, there is no obvious reduction peak for the cyclic voltammogram of CN/FTO-520 film checked without CO_2 . After purging CO_2 , one reduction peak appears at around $-0.25 \text{ V}_{\text{RHE}}$; it indicates that CO_2 can be reduced by CN/FTO-520 film. The potential of $-0.35 \text{ V}_{\text{RHE}}$ was selected for CO_2 reduction as shown in Figure 9b. The corresponding GC data and the production yields are shown in Figure 9c,d. For CN/FTO-520 film, the current slightly decreases as the time going on. Two main products of formaldehyde and ethanol are obtained. The concentrations of HCHO and EtOH are 118.6 and 47.19 μM , respectively. The production of EtOH could be caused by the low pH of the electrolyte. The electrolyte with low pH can support more protons which are used for the formation of EtOH.

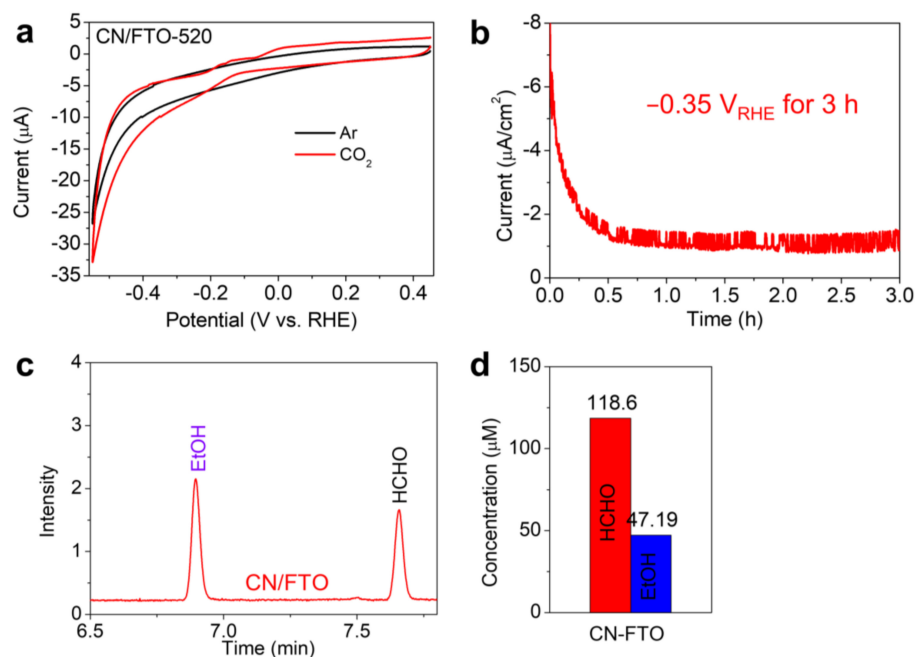


Figure 9. (a) Cyclic voltammograms of CN/FTO-520 using Ar-saturated and CO_2 -saturated 0.5 M KCl electrolyte. (b) I-t curve for CN/FTO-520 photoelectrochemical CO_2 reduction was recorded at -0.8 V for 3 h in CO_2 -saturated 0.5 M KCl under 1 sun light illumination. (c) GC spectra and (d) the corresponding product concentration for photoelectrochemical CO_2 reduction by CN/FTO-520 films in CO_2 -saturated 0.5 M KCl solution at $-0.35 \text{ V}_{\text{RHE}}$ for 3 h.

3. Materials and Experiments

3.1. Materials and Chemicals

Melamine ($C_3H_6N_6$, 99%, Aldrich, Seoul, Korea), Sodium sulfate (Na_2SO_4 , $\geq 99.0\%$, Sigma, Seoul, Korea), potassium bicarbonate ($KHCO_3$, 99.7%, Sigma-Aldrich, Seoul, Korea), and potassium chloride (KCl , $\geq 99.0\%$, Sigma-Aldrich, Seoul, Korea) were used without further purification. The aqueous solutions used in this work were prepared with deionized water which was further purified by a Millipore Milli-Q IQ 7000 purification system (resistivity $\geq 18.2 M\Omega \cdot cm$ at 25 °C, total organic carbon (TOC) < 2.4 ppb). The commercial fluorine-doped tin oxide (FTO) coated glasses (Pilkington FTO glass-TEC 8, 6~9 ohm/sq) were cleaned with ethanol, acetone and deionized water in sonication bath (Hwashin, Powersonic 410, Seoul, Korea) each for 10 min and dried by N_2 flowing for using. The as-received Nafion 117 (Du Pont, Seoul, Korea) membrane was cut into rectangular pieces (2.7 cm \times 3.5 cm). Firstly, the membrane pieces were boiled in 3 wt% H_2O_2 for 1 h at 90 °C and submerged in deionized water for 15 min at room temperature. Then the membrane pieces were sunk in 0.5 M H_2SO_4 for 3 h at 90 °C and submerged in distilled water for 15 min at room temperature. Finally, the membrane pieces were submerged in deionized water for 3 h at 90 °C and washed by deionized water for 3 times. After the pretreatment the membrane pieces are stored in deionized water for the later experiments.

3.2. Preparation of *g*- C_3N_4 Film on FTO (CN/FTO)

The CN/FTO films were prepared by a simple thermal vapor condensation method. 7.0 g melamine was put in the glass bottle (Bottle diameter–Height–Mouth inner diameter = 4.2 \times 8.0 \times 3.0 cm, SamwooKurex, Seoul, Korea) and covered by one piece of FTO glass (5.0 cm \times 5.0 cm). Then put them in the Muffle box furnace for heating at 520, 550, and 600 °C for 4 h with the increasing ramp of ca. 2 °C/min. It was cooled to room temperature in the furnace by the ambient environment. The *g*- C_3N_4 films on FTO glass (CN/FTO) were obtained at 520, 550, and 600 °C and denoted as CN/FTO-520, CN/FTO-550, and CN/FTO-600, respectively. The bulk *g*- C_3N_4 grains obtained at 520, 550, and 600 °C, with faint yellow color, were ground to fine powder by the pestle and mortar, which were denoted as CN-520, CN-550, and CN-600, respectively.

3.3. Characterization

X-ray diffraction (XRD, Cu $K\alpha$ radiation with $\lambda = 0.154056$ nm, Rigaku miniFlex-II desktop, Tokyo, Japan) patterns were measured to determine the crystallinity and crystal structure of the films and powders. Top-view and cross-sectional morphologies of the films were determined by using a field emission scanning electron microscope (FE-SEM, JEOL JSM-7600F) operated at 20 kV with energy-dispersive spectroscopy (EDS, INCA X-sight, Oxford Instruments, High Wycombe, UK). Atomic force microscopy (AFM) measurements were carried out for thin films in a tapping mode using a Park System NX10. The XEI program was used to convert acquired data into an image and to perform various analyses. Transmittance and diffuse reflectance spectra (DRS) of the films were recorded on a Varian Cary 5000 UV-vis-NIR spectrophotometer. DRS spectra were recorded using an integrating sphere and $BaSO_4$ as a reference. Attenuated total reflectance Fourier transform infrared spectroscopy (ATR-FTIR, Thermo Nicolet Avatar 330 FT-IR with ZnSe crystal) was checked for studying the detail chemical structures of the powder and films samples. The diffuse reflectance spectra were converted into the Kubelka-Munk (K-M) form. Transmission electron microscope (TEM, JEOL JEM-2100 F operating at 200 kV) with EDS was applied to characterize the exact composition of particles on CN/FTO film after the electrochemical CO_2 reduction. X-ray photoelectron spectroscopy (XPS, monochromator Al $K\alpha$ X-ray source, AXIS Ultra, Manchester, UK) was used to determine the atomic state in the films by measuring the binding energy. Time-resolved photoluminescence (TRPL) measurement was carried out using a confocal microscope (MicroTime-200, Picoquant, Germany) with a 40 \times objective. The lifetime measurements were performed at the Korea Basic Science Institute (KBSI), Daegu Center, Korea. A single-mode pulsed diode laser (375 nm with

30 ps pulse width and 5 μ W power) was used as an excitation source. A dichroic mirror (Z375RDC, AHF, Mainz, Germany), a long pass filter (HQ405lp, AHF, Mainz, Germany), a 75 μ m pinhole, a bandpass filter (470 ± 20 nm) and an avalanche photodiode detector (PDM series, MPD, Berlin, Germany) were used to collect emission photons from the samples. TRPL images consisted of 200×200 pixels were recorded using the time-tagged time-resolved data acquisition method. The acquisition time of each pixel was 1 ms. Exponential fitting for the obtained PL decays was accomplished using the Symphotime-64 software (Ver. 2.2, Berlin, Germany).

3.4. Photoelectrochemical Measurements

Photoelectrochemical measurements were conducted using a potentiostat (VSP, Bio-logics, Seyssinet-Pariset, France) in a conventional three-electrode system in a V-style with a quartz window cell at room temperature under 1 sun (Asahi HAL-320 solar simulator, AM1.5G, Class A) illumination, employing a coiled Pt wire and an Ag/AgCl electrode as the counter and reference electrodes, respectively. A 1 sun checker CS-20 was used to determine the light intensity to 1 sun. The potentials reported in this work were converted to the reversible hydrogen electrode (RHE) according to the following equation [31]. $E_{\text{RHE}} = E_{\text{Ag/AgCl}} + E^0_{\text{Ag/AgCl}} + 0.0591 \times \text{pH}$. In this equation, $E_{\text{Ag/AgCl}}$ is the experimental potential measured versus Ag/AgCl (3 M NaCl) reference electrode. $E^0_{\text{Ag/AgCl}}$ is the potential of Ag/AgCl (3 M NaCl) versus normal hydrogen electrode (NHE), i.e., 0.209 V. E_{RHE} is the converted potential versus RHE. The current–potential (I–V) curve was measured in 0.5 M Na_2SO_4 aqueous solution (pH 6.3) from +1.5 V to -0.25 V vs. RHE using linear sweep voltammetry (LSV) with a scan rate of 10 mV s^{-1} with chopped light (on/off cycles of 1 s). To know the electrochemical stability of CN/FTO film, the cyclic voltammetry experiment was carried out for 10 cycles for 1.58 V to -0.22 V vs. RHE. Photocurrent stabilities were studied by measuring the photocurrent produced under 1 sun light illumination at 1.18 V and 0.38 V vs. RHE for 1 h. Electrochemical impedance spectroscopy (EIS) was conducted in 0.5 M Na_2SO_4 using a VSP potentiostat. The frequency was set from 100 kHz to 50 mHz at open-circuit potential (E_{oc}) and the amplitude was 10 mV.

3.5. Electrochemical and Photoelectrochemical CO_2 Reduction

The electrochemical or photoelectrochemical CO_2 reduction was carried out using the same home-made quartz cell with two half chambers and Nafion 117 film between as shown in Figure 10. The exposed area of working and counter electrode in the electrolyte is about 1.13 cm^2 . 0.5 M KHCO_3 or 0.5 M KCl solution was used as electrolyte. The CO_2 was purging with a speed of 10 sccm. The pH values of the CO_2 -saturated 0.5 M KHCO_3 and the CO_2 -saturated 0.5 M KCl solutions are 7.6 and 4.1, respectively. The liquid products in solution were checked by 7890B series GC-FID (Agilent Technologies, Seoul, South Korea) equipped with a DB-624 column ($60 \text{ m} \times 250 \mu\text{m} \times 1.4 \mu\text{m}$) and Stratum Purge & Trap (TELEDYNE TEKMAR, Mason, OH, United States). Quantities of 10 mL of electrolyte samples containing salts were injected into the purge & trap instrument.

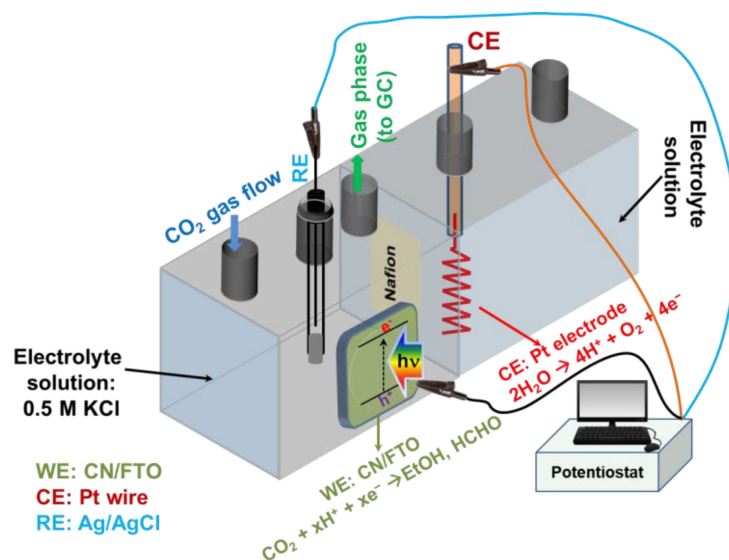


Figure 10. A schematic representation of the photoelectrochemical cell for CO_2 reduction. WE: working electrode; CE: counter electrode, coiled Pt wire; RE: reference electrode, Ag/AgCl with 3.0 M NaCl.

4. Conclusions

In this work, thin $g\text{-C}_3\text{N}_4$ films were synthesized by the simple thermal condensation method at different heating temperatures. All films show photoanodic and photocathodic behaviors. Especially, the film obtained at $520\text{ }^\circ\text{C}$ shows the best cathodic photocurrent performance due to the high thickness with the longest average lifetime of the photo-excited electrons. The CN/FTO-520 was selected for CO_2 reduction. The CO_2 can be electrochemically reduced into formaldehyde ($54.6\text{ }\mu\text{M/h}$) in the liquid product when using the basic electrolyte (CO_2 -saturated KHCO_3). When using the acidic electrolyte (CO_2 -saturated KCl), the CO_2 can be photoelectrochemically reduced into formaldehyde ($39.5\text{ }\mu\text{M/h}$) and ethanol ($15.7\text{ }\mu\text{M/h}$). Therefore, the acidic condition is good for the formation of ethanol product by $g\text{-C}_3\text{N}_4$ film. The pure $g\text{-C}_3\text{N}_4$ film can be used for CO_2 reduction to different value-added liquid hydrocarbons products via electrochemical or photoelectrochemical ways. This work could give a supporting for the preparation and modification of the $g\text{-C}_3\text{N}_4$ film for CO_2 reduction.

Supplementary Materials: The following supporting information can be downloaded at: <https://www.mdpi.com/article/10.3390/catal12111399/s1>, Figure S1: SEM and AFM images of the bare FTO glass; Figure S2: SEM-EDS of the CN/FTO-520 film; Figure S3: PL lifetime decay curves and their fitted curves; Figure S4: SEM images and XRD, STEM-EDS of CN/FTO-520 film after electrochemical CO_2 reduction; Table S1: Fitting results of PL lifetime decay curves and their corresponding average lifetime.

Author Contributions: Conceptualization, J.Y.Z. and Y.S.K.; methodology, J.Y.Z.; validation, J.Y.Z. and A.U.P.; formal analysis, A.U.P.; investigation, J.Y.Z.; resources, J.Y.Z.; data curation, J.Y.Z.; writing—original draft preparation, J.Y.Z.; writing—review and editing, A.U.P. and Y.S.K.; visualization, J.Y.Z.; supervision, Y.S.K.; project administration, J.Y.Z. and Y.S.K. All authors have read and agreed to the published version of the manuscript.

Funding: This research was supported by the Leader Project at Korea Institute of Energy Technology (KENTECH) funded by the Ministry of Science and ICT through the National Research Foundation of Korea (No. 2020R1A3B3079715), the National Natural Science Foundation of China (grant no. 51902292), the China Postdoctoral Science Foundation (grant no. 2019M662525) and the postdoctoral research grant in Henan Province (grant no. 19030019).

Data Availability Statement: The data presented in this study are available on request from the corresponding author.

Acknowledgments: This research was supported by the Leader Project at Korea Institute of Energy Technology (KENTECH) funded by the Ministry of Science and ICT through the National Research Foundation of Korea (No. 2020R1A3B3079715), the National Natural Science Foundation of China (grant no. 51902292), the China Postdoctoral Science Foundation (grant no. 2019M662525) and the post-doctoral research grant in Henan Province (grant no. 19030019).

Conflicts of Interest: The authors declare no conflict of interest.

References

1. Qiao, J.; Liu, Y.; Hong, F.; Zhang, J. A Review of Catalysts for the Electroreduction of Carbon Dioxide to Produce Low-Carbon Fuels. *Chem. Soc. Rev.* **2014**, *43*, 631–675. [[CrossRef](#)] [[PubMed](#)]
2. Wang, X.X.; Duan, Y.H.; Zhang, J.F.; Tan, Y.S. Catalytic Conversion of CO₂ into High Value-Added Hydrocarbons over Tandem Catalyst. *J. Fuel Chem. Technol.* **2022**, *50*, 538–563. [[CrossRef](#)]
3. Sangiorgi, N.; Tuci, G.; Sanson, A.; Peruzzini, M.; Giambastiani, G. Metal-Free Carbon-Based Materials for Electrocatalytic and Photo-Electrocatalytic CO₂ Reduction. *Rend. Lincei Sci. Fis. Nat.* **2019**, *30*, 497–513. [[CrossRef](#)]
4. Ong, W.J.; Tan, L.L.; Ng, Y.H.; Yong, S.T.; Chai, S.P. Graphitic Carbon Nitride (g-C₃N₄)-Based Photocatalysts for Artificial Photosynthesis and Environmental Remediation: Are We a Step Closer to Achieving Sustainability? *Chem. Rev.* **2016**, *116*, 7159–7329. [[CrossRef](#)] [[PubMed](#)]
5. Jia, C.; Yang, L.; Zhang, Y.; Zhang, X.; Xiao, K.; Xu, J.; Liu, J. Graphitic Carbon Nitride Films: Emerging Paradigm for Versatile Applications. *ACS Appl. Mater. Interfaces* **2020**, *12*, 53571–53591. [[CrossRef](#)]
6. Hasija, V.; Patial, S.; Singh, P.; Nguyen, V.-H.; Le, Q.V.; Thakur, V.K.; Hussain, C.M.; Selvasembian, R.; Huang, C.-W.; Thakur, S.; et al. Photocatalytic Inactivation of Viruses Using Graphitic Carbon Nitride-Based Photocatalysts: Virucidal Performance and Mechanism and Mechanism. *Catalysts* **2021**, *11*, 1448. [[CrossRef](#)]
7. Ng, S.; Jie, F.; Ong, W. Solar-Powered Chemistry: Engineering Low-Dimensional Carbon Nitride-Based Nanostructures for Selective CO₂ Conversion to C₁-C₂ Products. *InfoMat* **2022**, *4*, e12279. [[CrossRef](#)]
8. Martin, D.J.; Reardon, P.J.T.; Moniz, S.J.A.; Tang, J. Visible Light-Driven Pure Water Splitting by a Nature-Inspired Organic Semiconductor-Based System. *J. Am. Chem. Soc.* **2014**, *136*, 12568–12571. [[CrossRef](#)]
9. Wang, Y.; Wang, X.; Antonietti, M. Polymeric Graphitic Carbon Nitride as a Heterogeneous Organocatalyst: From Photochemistry to Multipurpose Catalysis to Sustainable Chemistry. *Angew. Chem.-Int. Ed.* **2012**, *51*, 68–89. [[CrossRef](#)]
10. Cao, S.; Yu, J. G-C₃N₄-Based Photocatalysts for Hydrogen Generation. *J. Phys. Chem. Lett.* **2014**, *5*, 2101–2107. [[CrossRef](#)]
11. Thomas, A.; Fischer, A.; Goettmann, F.; Antonietti, M.; Müller, J.O.; Schlögl, R.; Carlsson, J.M. Graphitic Carbon Nitride Materials: Variation of Structure and Morphology and Their Use as Metal-Free Catalysts. *J. Mater. Chem.* **2008**, *18*, 4893–4908. [[CrossRef](#)]
12. Dong, G.; Zhang, Y.; Pan, Q.; Qiu, J. A Fantastic Graphitic Carbon Nitride (g-C₃N₄) Material: Electronic Structure, Photocatalytic and Photoelectronic Properties. *J. Photochem. Photobiol. C Photochem. Rev.* **2014**, *20*, 33–50. [[CrossRef](#)]
13. Patnaik, S.; Martha, S.; Acharya, S.; Parida, K.M. An Overview of the Modification of G-C₃N₄ with High Carbon Containing Materials for Photocatalytic Applications. *Inorg. Chem. Front.* **2016**, *3*, 336–347. [[CrossRef](#)]
14. Cao, S.; Low, J.; Yu, J.; Jaroniec, M. Polymeric Photocatalysts Based on Graphitic Carbon Nitride. *Adv. Mater.* **2015**, *27*, 2150–2176. [[CrossRef](#)]
15. De Brito, J.F.; Corradini, P.G.; Silva, A.B.; Mascaro, L.H. Reduction of CO₂ by Photoelectrochemical Process Using Non-Oxide Two-Dimensional Nanomaterials—A Review. *ChemElectroChem* **2021**, *8*, 4305–4320. [[CrossRef](#)]
16. Sagara, N.; Kamimura, S.; Tsubota, T.; Ohno, T. Photoelectrochemical CO₂ Reduction by a P-Type Boron-Doped g-C₃N₄ Electrode under Visible Light. *Appl. Catal. B Environ.* **2016**, *192*, 193–198. [[CrossRef](#)]
17. Pawar, A.U.; Pal, U.; Zheng, J.Y.; Kim, C.W.; Kang, Y.S. Thermodynamically Controlled Photo-Electrochemical CO₂ Reduction at Cu/RGO/PVP/Nafion Multi-Layered Dark Cathode for Selective Production of Formaldehyde and Acetaldehyde. *Appl. Catal. B Environ.* **2022**, *303*, 120921. [[CrossRef](#)]
18. Liu, J.; Shi, H.; Shen, Q.; Guo, C.; Zhao, G. A Biomimetic Photoelectrocatalyst of Co-Porphyrin Combined with a g-C₃N₄ Nanosheet Based on π - π Supramolecular Interaction for High-Efficiency CO₂ Reduction in Water Medium. *Green Chem.* **2017**, *19*, 5900–5910. [[CrossRef](#)]
19. Xu, Y.; Wang, S.; Yang, J.; Han, B.; Nie, R.; Wang, J.; Dong, Y.; Yu, X.; Wang, J.; Jing, H. Highly Efficient Photoelectrocatalytic Reduction of CO₂ on the Ti₃C₂/g-C₃N₄ Heterojunction with Rich Ti³⁺ and Pyri-N Species. *J. Mater. Chem. A* **2018**, *6*, 15213–15220. [[CrossRef](#)]
20. Wang, Q.; Wang, X.; Yu, Z.; Jiang, X.; Chen, J.; Tao, L.; Wang, M.; Shen, Y. Artificial Photosynthesis of Ethanol Using Type-II g-C₃N₄/ZnTe Heterojunction in Photoelectrochemical CO₂ Reduction System. *Nano Energy* **2019**, *60*, 827–835. [[CrossRef](#)]
21. Eid, K.; Sliem, M.H.; Jlassi, K.; Eldesoky, A.S.; Abdo, G.G. Precise Fabrication of Porous One-Dimensional GC₃N₄ Nanotubes Doped with Pd and Cu Atoms for Efficient CO Oxidation and CO₂ Reduction. *Inorg. Chem. Commun.* **2019**, *107*, 107460. [[CrossRef](#)]
22. Xia, X.; Hu, X.D.; Tarek, M.; Saravanan, P.; Alqadhi, R. Tailoring the Properties of G-C₃N₄ with CuO for Enhanced Photoelectrocatalytic CO₂ Reduction to Methanol. *J. CO₂ Util.* **2020**, *40*, 101222. [[CrossRef](#)]
23. Papailias, I.; Giannakopoulou, T.; Todorova, N.; Demotikali, D.; Vaimakis, T.; Trapalis, C. Effect of Processing Temperature on Structure and Photocatalytic Properties of G-C₃N₄. *Appl. Surf. Sci.* **2015**, *358*, 278–286. [[CrossRef](#)]

24. Kim, S.; Bark, C.W. Effect of Surface Treatment by Chemical-Mechanical Polishing for Transparent Electrode of Perovskite Solar Cells. *Energies* **2020**, *13*, 585. [[CrossRef](#)]
25. Zheng, J.Y.; Kim, C.W.; Pawar, A.U.; Kang, Y.S. Fabrication of P-Cu₂O/n-Bi-WO₃ Heterojunction Thin Films: Optical and Photoelectrochemical Properties. *New J. Chem.* **2017**, *41*, 755–762. [[CrossRef](#)]
26. Kumar, P.; Vahidzadeh, E.; Thakur, U.K.; Kar, P.; Alam, K.M.; Goswami, A.; Mahdi, N.; Cui, K.; Bernard, G.M.; Michaelis, V.K.; et al. C₃N₅: A Low Bandgap Semiconductor Containing an Azo-Linked Carbon Nitride Framework for Photocatalytic, Photovoltaic and Adsorbent Applications. *J. Am. Chem. Soc.* **2019**, *141*, 5415–5436. [[CrossRef](#)]
27. Gashi, A.; Parmentier, J.; Fioux, P.; Marsalek, R. Tuning the C/N Ratio of C-Rich Graphitic Carbon Nitride (g-C₃N₄) Materials by the Melamine/Carboxylic Acid Adduct Route. *Chem.-Eur. J.* **2022**, *28*, e202103605. [[CrossRef](#)]
28. Dong, G.; Zhao, K.; Zhang, L. Carbon Self-Doping Induced High Electronic Conductivity and Photoreactivity of g-C₃N₄. *Chem. Commun.* **2012**, *48*, 6178–6180. [[CrossRef](#)]
29. Zhang, Z.; Liu, K.; Feng, Z.; Bao, Y.; Dong, B. Hierarchical Sheet-on-Sheet ZnIn₂S₄/g-C₃N₄ Heterostructure with Highly Efficient Photocatalytic H₂ Production Based on Photoinduced Interfacial Charge Transfer. *Sci. Rep.* **2016**, *6*, 19221. [[CrossRef](#)]
30. Zhang, Z.; Huang, J.; Zhang, M.; Yuan, Q.; Dong, B. Ultrathin Hexagonal SnS₂ Nanosheets Coupled with G-C₃N₄ Nanosheets as 2D/2D Heterojunction Photocatalysts toward High Photocatalytic Activity. *Appl. Catal. B Environ.* **2015**, *163*, 298–305. [[CrossRef](#)]
31. Zheng, J.Y.; Song, G.; Hong, J.; Van, T.K.; Pawar, A.U.; Kim, D.Y.; Kim, C.W.; Haider, Z.; Kang, Y.S. Facile Fabrication of WO₃ Nanoplates Thin Films with Dominant Crystal Facet of (002) for Water Splitting. *Cryst. Growth Des.* **2014**, *14*, 6057–6066. [[CrossRef](#)]
32. Yan, S.C.; Li, Z.S.; Zou, Z.G. Photodegradation of Rhodamine B and Methyl Orange over Boron-Doped g-C₃N₄ under Visible Light Irradiation. *Langmuir* **2010**, *26*, 3894–3901. [[CrossRef](#)]
33. Chen, L.; Yan, R.; Oschatz, M.; Jiang, L.; Antonietti, M.; Xiao, K. Ultrathin 2D Graphitic Carbon Nitride on Metal Films: Underpotential Sodium Deposition in Adlayers for Sodium-Ion Batteries. *Angew. Chem.-Int. Ed.* **2020**, *59*, 9067–9073. [[CrossRef](#)]
34. Dong, F.; Wu, L.; Sun, Y.; Fu, M.; Wu, Z.; Lee, S.C. Efficient Synthesis of Polymeric G-C₃N₄ Layered Materials as Novel Efficient Visible Light Driven Photocatalysts. *J. Mater. Chem.* **2011**, *21*, 15171–15174. [[CrossRef](#)]
35. Xu, M.; Han, L.; Dong, S. Facile Fabrication of Highly Efficient G-C₃N₄/Ag₂O Heterostructured Photocatalysts with Enhanced Visible-Light Photocatalytic Activity. *ACS Appl. Mater. Interfaces* **2013**, *5*, 12533–12540. [[CrossRef](#)]
36. Bian, J.; Li, Q.; Huang, C.; Li, J.; Guo, Y.; Zaw, M.; Zhang, R.Q. Thermal Vapor Condensation of Uniform Graphitic Carbon Nitride Films with Remarkable Photocurrent Density for Photoelectrochemical Applications. *Nano Energy* **2015**, *15*, 353–361. [[CrossRef](#)]
37. Wei, X.; Jiang, H.; Liu, Z. Liquid-Based Growth of Polymeric Carbon Nitride Films and Their Extraordinary Photoelectrocatalytic Activity. *RSC Adv.* **2016**, *6*, 81372–81377. [[CrossRef](#)]
38. Liu, J.; Wang, H.; Chen, Z.P.; Moehwald, H.; Fiechter, S.; Van De Krol, R.; Wen, L.; Jiang, L.; Antonietti, M. Microcontact-Printing-Assisted Access of Graphitic Carbon Nitride Films with Favorable Textures toward Photoelectrochemical Application. *Adv. Mater.* **2015**, *27*, 712–718. [[CrossRef](#)]
39. Lv, X.; Cao, M.; Shi, W.; Wang, M.; Shen, Y. A New Strategy of Preparing Uniform Graphitic Carbon Nitride Films for Photoelectrochemical Application. *Carbon N. Y.* **2017**, *117*, 343–350. [[CrossRef](#)]
40. Wang, J.; Zhang, C.; Shen, Y.; Zhou, Z.; Yu, J.; Li, Y.; Wei, W.; Liu, S.; Zhang, Y. Environment-Friendly Preparation of Porous Graphite-Phase Polymeric Carbon Nitride Using Calcium Carbonate as Templates, and Enhanced. *J. Mater. Chem. A Mater. Energy Sustain.* **2015**, *3*, 5126–5131. [[CrossRef](#)]
41. Zhang, Y.; Schnepf, Z.; Cao, J.; Ouyang, S.; Li, Y.; Ye, J.; Liu, S. Biopolymer-Activated Graphitic Carbon Nitride towards a Sustainable Photocathode Material. *Sci. Rep.* **2013**, *3*, 2163. [[CrossRef](#)] [[PubMed](#)]
42. Wei, X.; Qiu, Y.; Duan, W.; Liu, Z. Cathodic and Anodic Photocurrents Generation from Melem and Its Derivatives. *RSC Adv.* **2015**, *5*, 26675–26679. [[CrossRef](#)]
43. Ye, L.; Chen, S. Fabrication and High Visible-Light-Driven Photocurrent Response of G-C₃N₄ Film: The Role of Thiourea. *Appl. Surf. Sci.* **2016**, *389*, 1076–1083. [[CrossRef](#)]
44. Jeong, H.; Kang, M.J.; Jung, H.; Kang, Y.S. Electrochemical CO₂ Reduction with Low Overpotential by a Poly(4-Vinylpyridine) Electrode for Application to Artificial Photosynthesis. *Faraday Discuss.* **2017**, *198*, 409–418. [[CrossRef](#)]
45. Li, Q.; Fu, J.; Zhu, W.; Chen, Z.; Shen, B.; Wu, L.; Xi, Z.; Wang, T.; Lu, G.; Zhu, J.J.; et al. Tuning Sn-Catalysis for Electrochemical Reduction of CO₂ to CO via the Core/Shell Cu/SnO₂ Structure. *J. Am. Chem. Soc.* **2017**, *139*, 4290–4293. [[CrossRef](#)]
46. Zhang, Y.; Chen, L.; Li, F.; Easton, C.D.; Li, J.; Bond, A.M.; Zhang, J. Direct Detection of Electron Transfer Reactions Underpinning the Tin-Catalyzed Electrochemical Reduction of CO₂ Using Fourier-Transformed Ac Voltammetry. *ACS Catal.* **2017**, *7*, 4846–4853. [[CrossRef](#)]
47. Chen, Y.; Kanan, M.W. Tin Oxide Dependence of the CO₂ Reduction Efficiency on Tin Electrodes and Enhanced Activity for Tin/Tin Oxide Thin-Film Catalysts. *J. Am. Chem. Soc.* **2012**, *134*, 1986–1989. [[CrossRef](#)]
48. Feaster, J.T.; Shi, C.; Cave, E.R.; Hatsukade, T.; Abram, D.N.; Kuhl, K.P.; Hahn, C.; Nørskov, J.K.; Jaramillo, T.F. Understanding Selectivity for the Electrochemical Reduction of Carbon Dioxide to Formic Acid and Carbon Monoxide on Metal Electrodes. *ACS Catal.* **2017**, *7*, 4822–4827. [[CrossRef](#)]